JACS
JOURNAL OF THE AMERICAN CHEMICAL SOCIETY
Article
pubs.acs.org/JACS

Synthesis and Characterization of Quarteranthene: Elucidating the Characteristics of the Edge State of Graphene Nanoribbons at the Molecular Level

Akihito Konishi,[†] Yasukazu Hirao,[†] Kouzou Matsumoto,[†] Hiroyuki Kurata,[†] Ryohei Kishi,[‡] Yasuteru Shigeta,[‡] Masayoshi Nakano,[‡] Kazuya Tokunaga,[∥,§] Kenji Kamada,[∥,§] and Takashi Kubo*[,†]

[†]Department of Chemistry, Graduate School of Science, Osaka University, Toyonaka, Osaka 560-0043, Japan

[‡]Department of Materials Engineering Science, Graduate School of Engineering Science, Osaka University, Toyonaka, Osaka 560-8531, Japan

[∥]Research Institute for Ubiquitous Energy Devices, National Institute of Advanced Industrial Science and Technology (AIST), AIST Kansai Center, Ikeda, Osaka 563-8577, Japan

[§]Department of Chemistry, Graduate School of Science and Technology, Kwansei Gakuin University, Sanda, Hyogo 669-1337, Japan

Supporting Information

ABSTRACT: The characteristics of the edge state, which is a peculiar magnetic state in zigzag-edged graphene nanoribbons (ZGNRs) that originates from electron−electron correlation in an edge-localized π-state, are investigated by preparing and characterizing quarteranthene molecules. The molecular geometry that was determined from the X-ray analysis is consistent with a zigzag-edge-localized structure of unpaired electrons. The localized electrons are responsible for the peculiar magnetic (room-temperature ferromagnetic correlation), optical (the lowest-lying doubly excited state), and chemical (peroxide bond formation) behaviors. On the basis of these distinguishing properties and a careful consideration of the valence bonding, insight into the edge state of ZGNRs can be gained.

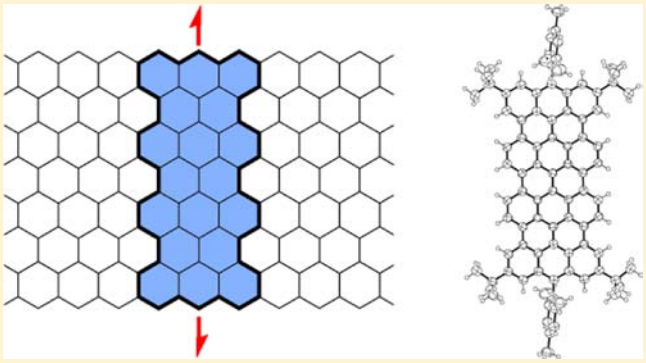

INTRODUCTION

Since the first characterization of graphene in 2004 by Geim and Novoselov,[1] research on graphene has boomed in the fields of physics, chemistry, and electronic device applications.[2] Currently, a central concern in this field is how graphene behaves when it is cut into nanoscale ribbons or flakes with distinct open edges.[3] An essential structure relevant to this concern is graphene nanoribbons (GNRs), which have peculiar electronic properties that are strongly influenced by the edge shape.[4−6] It has been suggested that zigzag-edged graphene nanoribbons (ZGNRs, Figure 1a) possess a localized nonbonding π-state around the zigzag edges, while armchair-edged GNRs (Figure 1b) do not have such a state. The localized nonbonding π-state, which can be approximately described as a spin-polarized state according to the broken-symmetry single-determinant approach to multielectron correlation among unpaired electrons on the zigzag edges, is predicted to yield specific magnetic activities in GNRs. This peculiar electron localization, along with the symmetry-broken spatial spin distribution in ZGNRs, is referred to as the "edge state",[5,6] and attempts have been made to observe the edge state using various experimental approaches.[7−13] In particular, scanning tunneling microscopy and spectroscopy (STM/S) approaches have achieved good evidence of the edge state around the zigzag edges in GNRs.[7,12,13]

These broad theoretical and experimental studies of the edge state have clearly demonstrated that the precise fabrication of edge structures in GNRs is one key to understanding the varied behaviors of the edge state.[5,6,12,14,15] Although GNRs can be prepared using chemical[3a,16,17] and lithographic methods[18,19] as well as through the unzipping of carbon nanotubes,[20,21] the synthesis of perfectly terminated GNRs with reliably controlled sizes has been in high demand,[22] and as such, the elucidation of the edge state at the molecular level has become increasingly important. Polycyclic aromatic hydrocarbons (PAHs) are possible candidates for this purpose, since they are structural components of GNRs with distinct edge structures and have been estimated to possess a spin state similar to those of GNRs.[23−26] With this in mind, we have focused on anthenes (Figure 1c), which are rectangular PAHs with both zigzag and armchair edges, as essential structural elements that induce the

Received: October 3, 2012
Published: January 7, 2013

   dx.doi.org/10.1021/ja309599m | J. Am. Chem. Soc. 2013, 135, 1430−1437

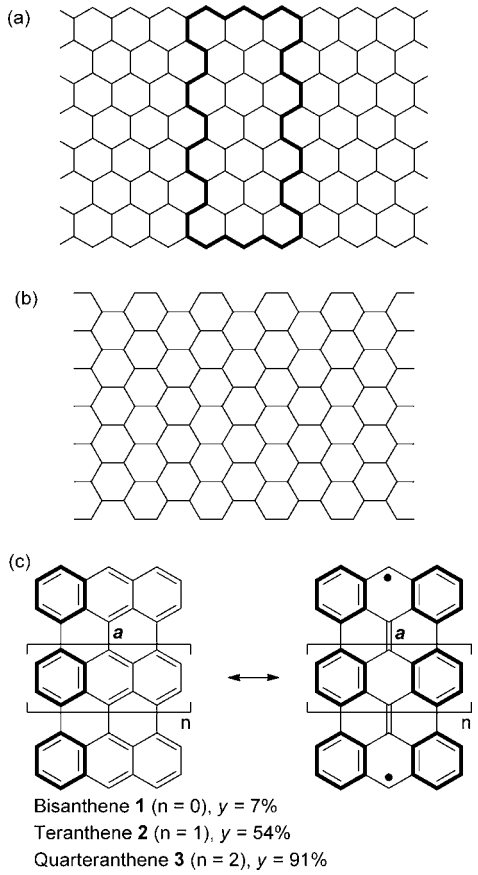

Figure 1. Chemical structure of GNRs and anthenes. (a) Zigzag-edged GNR (15.4 Å ribbon width). The bold line represents a quarteranthene (**3**) skeleton. (b) Armchair-edged GNR (14.5 Å ribbon width). (c) Resonance structure of anthenes. The amount of singlet biradical character (y) was calculated at the CASSCF(2,2)/6-31G level. The six-membered rings depicted by bold lines represent the Clar sextets.

edge state in GNRs. Our recent experimental and theoretical studies of teranthene (**2**) have afforded a glimpse of the edge state at the molecular level and have revealed that the spin-polarized state (singlet biradical state) is associated with the formation of aromatic sextets.[27,28] This spin-polarized state is also investigated in some π-conjugated small molecules having a quinoid skeleton,[29] and therefore characterizing anthene molecules in terms of singlet biradical character would be a reasonable approach to elucidate the characteristics of the edge state of ZGNRs.

Here, we report the explicit observation of the edge state using a larger anthene, quarteranthene (**3**), through organic synthesis and physical measurements. We first describe the stepwise synthesis of quarteranthene, and then the electron localization at the zigzag edges is demonstrated by the structural analysis, physical measurements, and chemical reactivity of **3**.

RESULTS

Synthesis of Quarteranthene. Scheme 1 displays the stepwise synthetic route to **3a** and **3b**. Lithiation of **4** followed by the coupling with (*Z*)-1,1′,5,5′-tetrachlorobianthrone[30] and a subsequent treatment with $SnCl_2$ in acetic acid gave **5**. Cyclization of **5** was carried out with KOH/quinoline to give a partially ring-closed quinone **6**.[31,32] Treatment of **6** with mesitylmagnesium bromide in the presence of $CeCl_3$[33] and subsequent reductive aromatization afforded the partially ring-closed hydrocarbons **7a** and **7b**. Cyclization of **7a** and **7b** with DDQ/$Sc(OTf)_3$ followed by $NEt_3/N_2H_4{\cdot}H_2O$ quench[34] gave **3a** and **3b** as bluish-black solids, respectively. Fortunately, we could obtain single crystals of **3a** suitable for X-ray crystallographic analysis by a careful recrystallization from an *o*-dichlorobenzene/mesitylene solution in a degassed sealed tube. The electronic absorption spectrum of **3a** in 1,2,4-trichlorobenzene had a low-energy band centered at 917 nm with a long tail up to 1300 nm (Figure S1 in SI). From the decay of the absorption bands, **3a** was determined to have a half-life of only 15 h at room temperature when exposed to air under room light.

Molecular Geometry. The X-ray crystallographic analysis of **3a** indicated two independent molecules (hereafter, molecules A and B) in the asymmetric unit, one of which is shown in Figure 2. Although there are small differences in the dihedral angles of the mesityl groups (ca. 65° for molecule A and ca. 78° for molecule B), no appreciable differences are observed in the quarteranthene rings. The mean width between the zigzag edges is 15.7 Å. In the packing diagram (Figure S2 in SI), molecules A and B alternately stack in a crossed manner with a mean interplanar distance of ∼3.46 Å to form a one-dimensional chain.

The geometry of **3a** determined from the X-ray analysis strongly suggests the localization of electrons at the zigzag edges. As shown in Figure 1c, the biradical resonance contribution shortens the *a* bonds by increasing their double-bond character. The mean length of the *a* bond in **3a** is 1.414(3) Å (Figure 3), which is considerably shorter than the corresponding bonds in teranthene[27] **2** (1.424(2) Å) and bisanthene[35] **1** (1.447(4) Å). This bond shortening trend is in line with the increase in singlet biradical character (y) estimated by the CASSCF(2,2)/6-31G calculation, which gave a significantly high LUMO occupation number of 0.91 for **3**, in contrast to 0.54 for **2** and 0.07 for **1**.[36,37] Furthermore, the harmonic oscillator model of aromaticity (HOMA) values,[38,39] which are geometry-based aromaticity indexes, indicated more benzenoid character for the peripheral six-membered rings (the bold benzene rings in the biradical structure in Figure 1c), as shown in Figure 3. These geometric findings suggest that the formation of aromatic sextets overwhelms the penalty for breaking one π-bond and pushes the resulting unpaired electrons out to the zigzag edges.

Magnetic Properties. The magnetic coupling of the edge-localized electrons in **3a** was estimated by performing SQUID measurements on a powdered sample (Figure 4). The measurement showed increasing susceptibility above 50 K. From careful fitting of the observed increase, the singlet−triplet energy gap ($\Delta E_{S\text{-}T}$), that is, the magnetic coupling strength, was determined to be 347 K (30 meV), which is comparable to the theoretical coupling strength of 25 meV calculated using a first-principles method for a 15-Å-wide GNR.[40] This very small $\Delta E_{S\text{-}T}$ indicates that **3a** is easily activated to a triplet state (a ferromagnetically correlated state) and that the population of the triplet species is ∼50% at room temperature.

The fluid toluene solution of **3b** (we used **3b** instead of **3a** for ESR measurements because **3a** becomes insoluble at low temperatures) at room temperature gave a featureless broad signal centered at g = 2.002 (Figure S4 in SI). The signal broadening would come from a large electron−electron dipole interaction within the molecule.[41] The signal intensity

dx.doi.org/10.1021/ja309599m | J. Am. Chem. Soc. 2013, 135, 1430−1437

Scheme 1. Stepwise Synthetic Route to Quarteranthenes 3a (Ar = Mesityl) and 3b (Ar = 4-*tert*-Butyl-*m*-xylyl)[a]

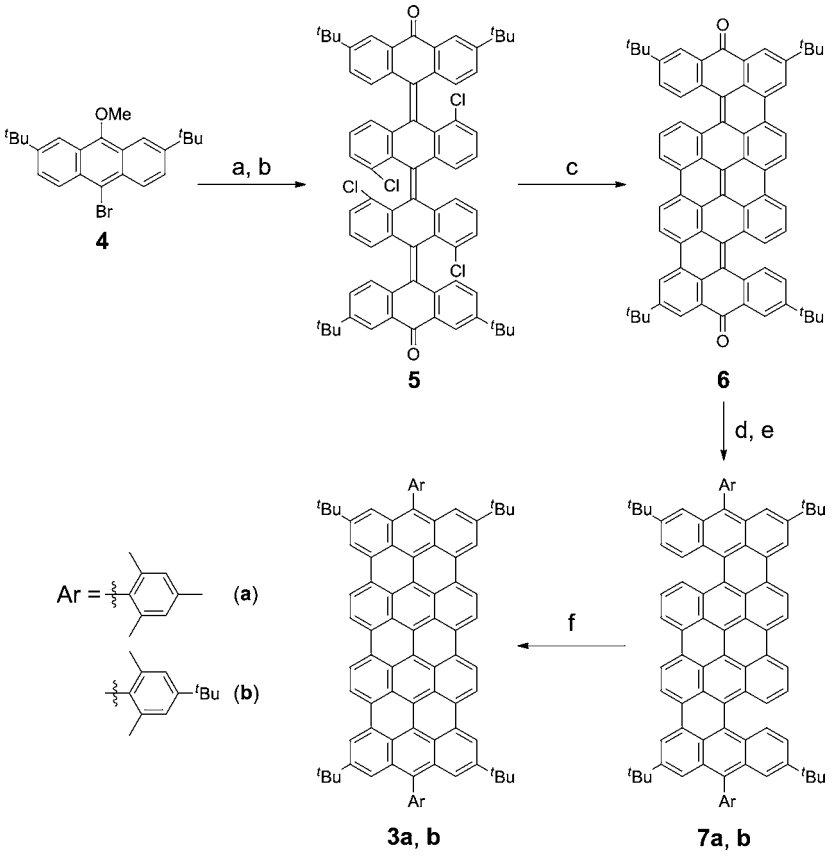

[a]Reagents and conditions: (a) ^{n}BuLi, then tetrachlorobianthrone. (b) $SnCl_2$, AcOH, 58% (2 steps). (c) KOH, quinolone, 36%. (d) ArMgBr, $CeCl_3$, THF. (e) $SnCl_2$, AcOH, 62% (**7a**, 2 steps), 64% (**7b**, 2 steps). (f) DDQ, $Sc(OTf)_3$, 43% (**3a**), 57% (**3b**).

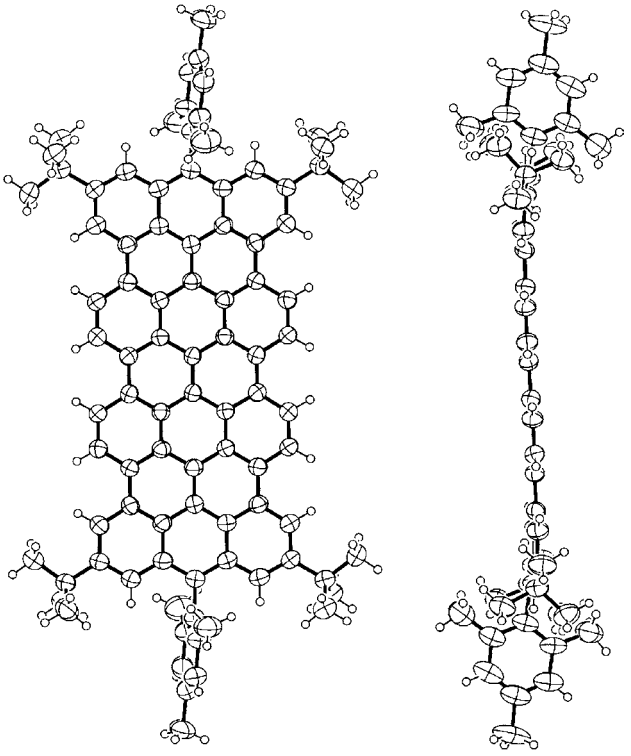

Figure 2. ORTEP drawings of **3a** at the 50% probability level: (left) top view and (right) side view.

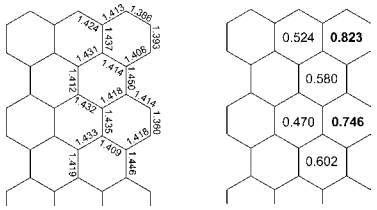

Figure 3. (Left) Mean bond lengths (Å) in the main core ring of **3a**, and (right) HOMA values of **3a**.

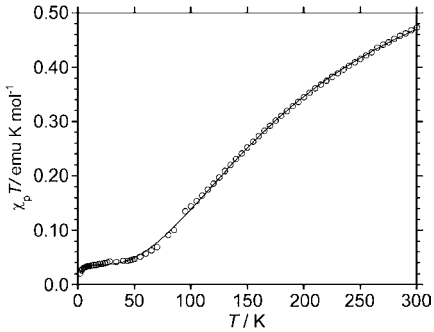

Figure 4. $\chi T-T$ plot for the powdered **3a**. The measured data are plotted as open circles. The line is the theoretical curve calculated using the alternating Heisenberg chain model with parameters of $2J_{intra}/k_B = -347$ K, $2J_{inter}/k_B = 2\alpha J_{intra}/k_B = -151$ K ($\alpha = 0.436$), impurity spin contamination =5.0%, $g = 2.002$, and diamagnetic susceptibility = -894.5×10^{-6} emu/mol.

dx.doi.org/10.1021/ja309599m | *J. Am. Chem. Soc.* 2013, 135, 1430−1437

decreased upon cooling to 230 K and its temperature dependency is consistent with the SQUID measurements. We could not discern ESR signals of the triplet species of **3b** in glassy toluene at 140 K, since a $\Delta M_s = \pm 1$ peak (peak-to-peak width, $\Delta H_{pp} \approx 1$ mT) would obscure the triplet species signal which should have a small D value (~0.7 mT based on the distance between the zigzag edges). The forbidden $\Delta M_s = \pm 2$ half-field signal also could not be observed. A triplet state signal at half-field is known to not be observable when there is a large separation between two electrons.[42]

Optical Properties. According to the SQUID measurements, the electronic absorption spectrum of **3a** measured at room temperature should be composed of absorption bands derived from triplet species as well as ground-state singlet species. In order to identify the bands of the singlet species, we performed variable-temperature measurements. The spectrum of **3b** at 303 K exhibited a low-energy band at 920 nm along with a shoulder band, while a new bathochromically shifted band along with isosbestic points was observed at 970 nm upon cooling to 183 K (Figure 5). Obviously, the bathochromically

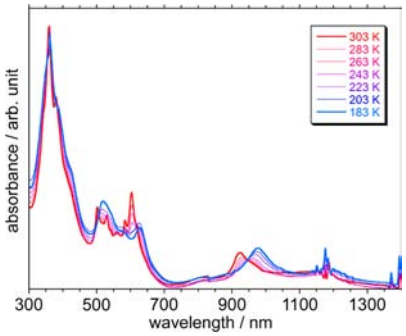

Figure 5. Electronic absorption spectra of **3b** in CH_2Cl_2 (3.6×10^{-5} M) for different temperatures.

shifted spectrum is derived from the ground state of quarteranthene. Interestingly, the spectra of the singlet and triplet species are quite similar, which is unusual, since most PAHs have totally different spectra in the singlet and triplet states.[43] The similarity of the spectra may indicate similar distributions of unpaired electrons around the zigzag edges in the singlet and triplet states. Indeed, the UB3LYP/6-31G* calculation gives almost identical distribution patterns (except for the spin orientation) of the unpaired electrons in the singlet and triplet state (Figure S7 in SI), where the unpaired electrons reside mostly on the zigzag edges.

The transition to the low-lying excited states should be related to the excitation of the edge-localized electrons. In order to assign the absorption bands of the singlet species, we performed a strongly contracted second-order n-electron valence state perturbation theory (NEVPT2) calculation that allows multielectron excitation.[44] The NEVPT2(8,8)/6-31G* calculation revealed that the first excited singlet state (S_1) of quarteranthene is a $2A_g$ state dominated by a HOMO, HOMO→LUMO, LUMO double excitation. The excitation energy from the ground state (S_0) to S_1 was estimated to be 1.32 eV (940 nm). The $S_0 \rightarrow S_1$ transition is one-photon-forbidden because of the parity ($g-g$ transition); consequently, the weak band of **3b** centered at around 1150 nm could be assigned to the transition to the forbidden state (the breakdown of the parity forbiddeness would come from a vibronic coupling between the $2A_g$ and $1B_{3u}$ (S_2) states). This assignment was confirmed by measuring the two-photon absorption (TPA), since a two-photon excitation into an A_g state is an allowed process. We could identify a broad band at around 2300 nm, which is the same excitation energy as that of the one-photon band around 1150 nm, in TPA measurements of a CS_2 solution of **3b** (Figure 6).[45] Thus, the weak band around 1150 nm is associated with the simultaneous excitation of the edge-localized electrons.

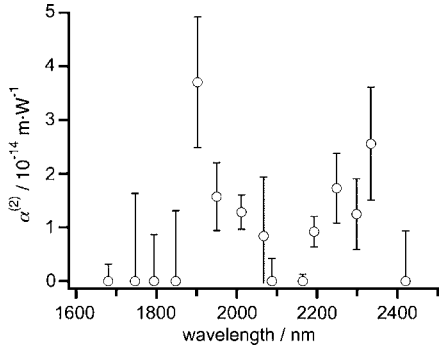

Figure 6. Two-photon absorption spectrum of a CS_2 solution of **3b** (1.1×10^{-3} M) under degassed condition at room temperature (296 K) measured by the femtosecond Z-scan method. $\alpha^{(2)}$ is the two-photon absorption coefficient.

The NEVPT2 calculation also indicated that the second excited singlet state (S_2) of quarteranthene is a $1B_{3u}$ state that possesses an almost pure HOMO→LUMO configuration, and the $S_0 \rightarrow S_2$ excitation energy and oscillator strength were estimated to be 1.39 eV (888 nm) and 0.33, respectively. The transition moment was parallel to the long molecular axis. Therefore, the band of moderate intensity observed at 980 nm for **3b** is assignable to the $S_0 \rightarrow S_2$ transition. Since the highest occupied natural orbital (HONO) and the lowest unoccupied natural orbital (LUNO) are distributed mainly on the zigzag edges (Figure 7), it can be concluded that the band is derived from electron transfer between the zigzag edges to afford a charge-resonance state.

Chemical Reactivity at the Zigzag Edges. The reactivity of quarteranthene toward oxygen is associated with the edge-localized electrons. A toluene solution of **3b** was allowed to stand exposed to air under dark conditions at 3 °C for several days (Figure 8a), which afforded an oxygen-adduct one-dimensional polymer (**8**) in a crystalline form. The structure of

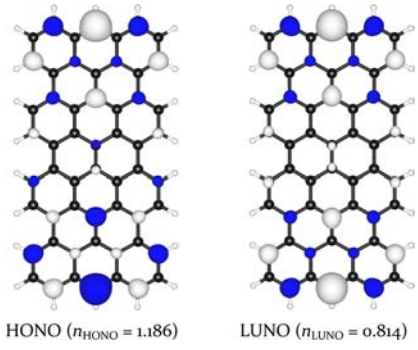

Figure 7. Isosurface maps and occupation numbers of HONO and LUNO obtained from the ground-state electron density calculated at the CASSCF(8,8)/6-31G* level of approximation. White/blue meshes represent the isosurfaces with contour values of +0.03/−0.03 au.

dx.doi.org/10.1021/ja309599m | J. Am. Chem. Soc. 2013, 135, 1430−1437

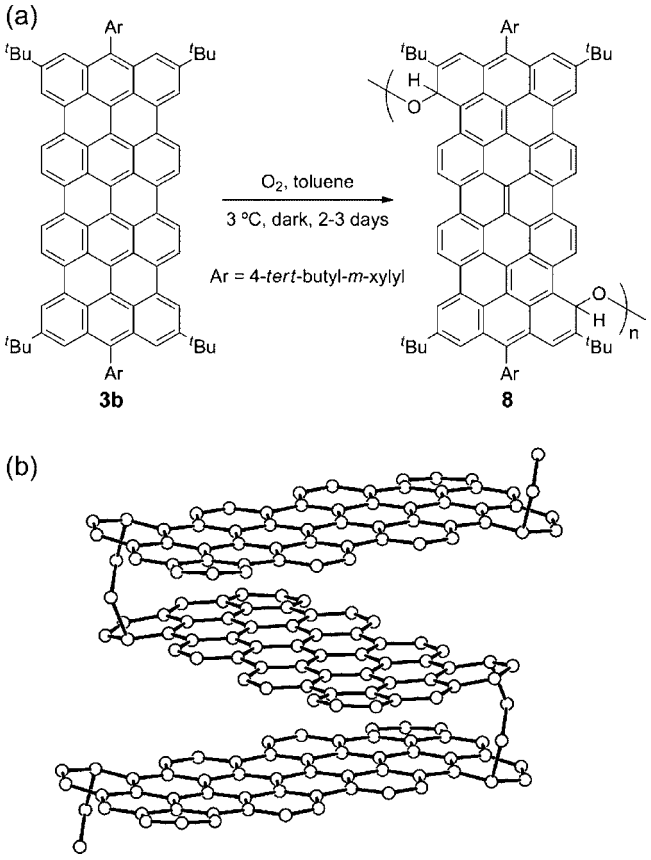

Figure 8. (a) Reaction of **3b** with oxygen. The most dominant Clar structure is drawn for **11** on the basis of the HOMA analysis. (b) X-ray structure of **8**. Ar, ^{t}Bu groups, and H atoms are omitted for clarity.

8 was determined by X-ray crystallographic analysis (Figure 8b). The oxygen molecule attacks a less-protected carbon atom with a large spin density around the zigzag edge, presumably via a radical mechanism, and forms a peroxide bond connecting the neighboring molecules. The HOMA analysis of **8** (Figure 9)

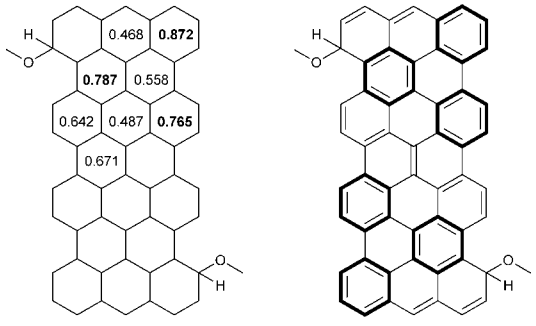

Figure 9. (Left) HOMA values and (right) the corresponding Clar structure of **8**.

clarified that the zigzag edges disappear after the oxygen attack, and, instead, a more stable PAH skeleton that is completely surrounded by armchair edges is generated. The zigzag edges in nanographene are well known to be thermodynamically unstable[46,47] and can be easily transformed into the more stable armchair edges by attacks by oxygen and various small molecules. The degradation process of the zigzag edges in **3b** may be a key element for clarifying the degradation mechanisms of ZGNRs.

DISCUSSION AND CONCLUSION

Based on the valence bond model shown in Figure 1c, anthenes are expected to behave as singlet biradical (spin-polarized) species, since the biradical canonical structures are reasonably stabilized by the formation of aromatic sextets when the Kekulé structures are transformed to the biradical structures. The contribution weight of the biradical structure in the ground state increases with the molecular size as a result of the cumulative increase in the number of aromatic sextets. Previous studies on bisanthene (**1**) and teranthene (**2**) revealed that bisanthene can be categorized as a nonmagnetic species, while teranthene lies at the onset of the edge state. In this article, we demonstrated that quarteranthene (**3**) possesses unpaired electrons localized at the zigzag edges by examining the molecular structure, magnetic and optical properties, and chemical behavior. Because the physical and chemical properties of quarteranthene are well explained by the edge localization of the unpaired electrons and because room-temperature ferromagnetic correlation was observed in the SQUID measurements, quarteranthene can be considered the minimal structural element of ZGNRs that still shows peculiar magnetic properties. The multispin correlation in ZGNRs, which is antiferromagnetic across the ribbon and ferromagnetic along the ribbon, could be simulated by aligning anthenes side by side.

The detection of the magnetic moment around the edges in ZGNRs has been a long-standing goal since it was first predicted by Fujita based on the Hubbard model calculation.[5] Although the spin polarization itself, which appears in broken-symmetry single-determinant calculations, is not experimentally observable in singlet systems, the concept of spin polarization is useful for analyzing the spatial spin correlation and thus can be used for predicting a real spin state realized under external perturbations. We found that the unpaired electrons in quarteranthene respond sharply to external perturbations such as heating, photoirradiation and chemical reaction, which means that quarteranthene has a prominent spin correlation in the ground state approximately described by the spin-polarized state and that the edge state indeed exists as an experimentally observable state.

By using quarteranthene, we are able to observe peculiar magnetic and optical properties relevant to the correlation of two unpaired electrons localized at the zigzag edges. For this reason quarteranthene is an ideal system for essentially understanding various behaviors of ZGNRs arising from the multispin correlation. Our findings may not only unveil the still unknown properties of ZGNRs but also pave the way to a bottom-up approach for producing spintronic, electronic, optical and magnetic devices based on molecular-sized nanographene materials.

EXPERIMENTAL SECTION

General. All experiments with moisture- or air-sensitive compounds were performed in anhydrous solvents under an argon atmosphere in well-dried glassware. Dried solvents were prepared by distillation under argon. Anhydrous ethanol was dried and distilled over Mg/I_2. THF was dried and distilled over sodium/benzophenone. Dichloromethane, toluene, and benzene were dried and distilled over calcium hydride. Column chromatography was performed with silica gel (Silica gel 60, Merck). Infrared spectra were recorded on a JASCO FT/IR-660M spectrometer. Electronic absorption spectrum was measured with a JASCO V-570 spectrometer. ^{1}H NMR spectra were obtained on JEOL EX-270, Bruker Mercury300, and JEOL GSX400 spectrometers. Positive EI, MALDI-TOF, and ESI mass spectra were

dx.doi.org/10.1021/ja309599m | J. Am. Chem. Soc. 2013, 135, 1430−1437

taken by using Shimadzu QP-5050, Shimadzu AXIMA-CFR, Applied Biosystems Japan Ltd. QSTAR Elite, and ThermoFisher Scientific LTQ ORBITRAP XL mass spectrometers, respectively. The high-resolution mass spectrum was analyzed by using Applied Biosystems Japan Ltd. Analyst QS 2.0 and ThermoXcalibur 2.1.0.1140 software. Data collection for X-ray crystal analysis was performed on a Rigaku/Varimax diffractometer (Mo Kα, λ = 0.71075 Å). The structure was solved with direct methods and refined with full-matrix least-squares (teXsan). Cyclic voltammetry measurement was conducted with a BAS CV-50W electrochemical analyzer. The cyclic voltammogram of **3a** (5×10^{-4} M) was recorded with a glassy carbon working electrode and a Pt counter electrode in *o*-dichlorobenzene containing 0.1 M Bu_4NClO_4 as supporting electrolyte. The experiment employed an $Ag/AgNO_3$ reference electrode and was done under a nitrogen atmosphere at room temperature. The temperature-dependent magnetic susceptibility was measured for randomly oriented polycrystalline samples of **3a** on a Quantum Design SQUID magnetometer MPMS-XL in the temperature range of 2−300 K. ESR spectra were measured in a toluene solution (1×10^{-4} M) with a JEOL JES-FE1X X-band spectrometer.

10,10′-((*Z*)-1,1′,5,5′-Tetrachlorobianthrone-10,10′-diylidene)bis(2,7-di-*tert*-butylanthracen-9(10*H*)-one) (5). A solution of *n*-butyllithium in hexane (1.6 M, 4.9 mL) was added to a solution of **4**[27] (2.92 g, 7.3 mmol) in ether (20 mL) at 0 °C under argon atmosphere. (*Z*)-1,1′,5,5′-Tetrachlorobianthrone (1.88 g, 3.6 mmol) and THF (15 mL) were added to the mixture after it was stirred at 0 °C for 15 min. The mixture was stirred for 2 days at 0 °C and then brought to room temperature and quenched with glacial acetic acid (2 mL). After solvents were evaporated from the mixture, $SnCl_2$ (3.10 g, 16 mmol) and glacial acetic acid (20 mL) were added to the residue. The mixture was refluxed for 3 days. After cooling, the crude product was filtered and recrystallized from hexane/acetone to give **8** as a yellow solid (2.31 g, 58%): mp (from EtOH/CH_2Cl_2) >300 °C; TLC (CH_2Cl_2:hexane, 1:1 v/v) R_f = 0.59; ^{1}H NMR (400 MHz, $CDCl_3$) δ 8.26 (d, J = 2.4 Hz, 2H), 8.25 (d, J = 2.0 Hz, 2H), 7.82 (d, J = 8.4 Hz, 2H), 7.45 (d, J = 8.4 Hz, 2H), 7.40 (dd, J = 7.6, 1.2 Hz, 2H), 7.35 (dd, J = 8.8, 2.4 Hz, 2H), 7.31 (dd, J = 8.0, 2.0 Hz, 2H), 7.27 (dd, J = 8.0, 1.2 Hz, 2H), 7.21 (dd, J = 8.0, 1.2 Hz, 2H), 7.09 (t, J = 7.6 Hz, 2H), 6.98−7.05 (m, 4H), 1.397 (s, 18H), 1.395 (s, 18H) ppm; IR (KBr) 3064 (w), 2963 (s), 2904 (m), 2868 (m), 1667 (s), 1602 (s), 1549 (m), 1484 (m), 1444 (s), 1364 (m), 1302 (m), 1248 (s), 1143 (s), 1120 (s), 969 (s) cm^{-1}; MS (MALDI) m/z [M]$^+$ 1097.2, [M+H]$^+$; analysis (calcd/found for $C_{72}H_{60}Cl_4O_2$) C 78.68/78.52, H 5.50/5.54.

3,7,16,20-Tetra-*tert*-butyldianthra[9,1-*fgv*;9,1-*qr*]bisanthene-5,18-dione (6). A solution of **5** (0.417 g, 0.380 mmol) and KOH (1.61g, 29 mmol) in quinoline (15 mL) was boiled at 190 °C under argon atmosphere for 2 h. After cooling, quinoline was distilled away under vacuum. The product was extracted with chloroform. The organic layer was washed with hydrochloric acid, water, and brine and dried over Na_2SO_4. The filtrate was evaporated, and the residue obtained was adsorbed by a small amount of silica gel. The mass was then put onto an alumina column for chromatography and eluted with CH_2Cl_2 and $CHCl_3$:CH_2Cl_2 (1:1 v/v) to give **6** as a reddish-purple solid (0.129 g, 36%): mp (from CH_2Cl_2) >300 °C; TLC (CH_2Cl_2) R_f = 0.56; ^{1}H NMR (300 MHz, $CDCl_3$) δ 9.18 (d, J = 1.5 Hz, 2H), 9.09 (d, J = 1.2 Hz, 2H), 8.85 (d, J = 9.6 Hz, 2H), 8.63(d, J = 9.0 Hz, 2H), 8.41−8.45 (m, 6H), 7.80 (d, J = 8.7 Hz. 2H), 7.31 (d, J = 6.6 Hz, 2H), 7.11 (dd, J = 8.7, 2.7 Hz, 2H), 1.75 (s, 18H), 1.36 (s, 18H) ppm; IR (KBr) 3069 (w), 2957 (s), 2903 (m), 2867 (m), 1654 (s), 1597 (s), 1567 (m), 1482 (m), 1362 (m), 1251 (s),1050 (w), 886 (w), 840 (m), 802 (s), 757 (s), 663 (m) cm^{-1}; MS (MALDI) m/z 952.5 [M] $^+$, 953.5 [M+H]$^+$; HRMS (ESI) m/z) [M+H]$^+$ calcd for $C_{72}H_{57}O_2$ 953.4353, found 953.4331.

3,7,16,20-Tetra-*tert*-butyl-5,18-diaryldianthra[9,1-*fg*;9,1-*qr*]bisanthene (7a and 7b). A solution of arylmagnesium bromide (6.7 mmol) in THF (10 mL) was added to a suspension of cerium trichloride (2.35 g, 7.2 mmol) in THF (40 mL) at 0 °C under an argon atmosphere, and the mixture was stirred for 1.5 h at that temperature. The mixture was further cooled to −40 to −50 °C, and then a solution of **6** (0.120 g, 0.126 mmol) in THF (10 mL) was added. The mixture was stirred for 2 h at the low temperature and quenched with aqueous NH_4Cl. The product was extracted with CH_2Cl_2, and the organic layer was washed with water and brine and dried over Na_2SO_4. The filtrate was evaporated, and the residue obtained was dissolved in anhydrous toluene (2 mL). $SnCl_2$ (0.30 g, 1.6 mmol) was added to the toluene solution and stirred for 15 min at room temperature under an argon atmosphere. After stirring, hexane was added to the reaction mixture, and the solution was poured onto hydrous (6%) alumina. The product was eluted with toluene: hexane (1:1 v/v) to give **7** as a reddish-purple solid (**7a**, R = methyl, 0.092 g,62%; **7b**, R = *tert*-butyl, 0.119 g, 64%).

3,7,16,20-Tetra-tert-butyl-5,18-dimesityldianthra[9,1-fg; 9,1-qr]bisanthene (7a): mp >300 °C; TLC (toluene:hexane, 1:1 v/v) R_f = 0.59; IR (KBr) 3066 (w), 2960 (s), 2864 (s), 1611 (w), 1587 (w), 1477 (m), 1460 (s), 1362 (s), 1256 (m), 942 (s), 849 (w) cm^{-1}; MS (MALDI) m/z 1159.3 [M+H]$^+$; HRMS (ESI) m/z [M]$^+$ calcd for $C_{90}H_{78}$ 1158.6098, found 1158.6109.

3,7,16,20-Tetra-tert-butyl-5,18-di(4-tert-butyl-2,6-dimethylphenyl)dianthra[9,1-fg;9,1-qr]bisanthene (7b): mp >300 °C; IR (KBr) 3066 (w), 2959 (s), 2910 (s), 2865 (s), 1588 (w), 1478 (m), 1459 (m), 1361 (m), 1258 (m), 958 (m), 803 (m) cm^{-1}; HRMS (ESI) m/z [M]$^+$ calcd for $C_{96}H_{90}$ 1242.7037, found 1242.7045.

2,6,13,17-Tetra-*tert*-butyl-4,15-dimesitylquarteranthene (3a). The precursor **7a** (0.091 g, 0.078 mmol), DDQ (0.093 g, 0.41 mmol), and $Sc(OTf)_3$ (0.276 g, 0.60 mmol) were dissolved in anhydrous toluene (20 mL), and the mixture was refluxed for 84 h under an argon atmosphere. After the mixture was cooled to room temperature, Et_3N (0.2 mL) and $N_2H_4{\cdot}H_2O$ (0.1 mL) were added to the mixture, and the mixture was stirred for 10 min at that temperature. The reaction mixture was poured onto hydrous (6%) alumina, and the product was eluted with toluene to give **3a** as a bluish-black solid (0.039 g, 43%). Single crystals of **3a** were obtained by recrystallization from a mesitylene/*o*-dichlorobenzene solution: mp (from mesitylene/*o*-dichlorobenzene) >300 °C; IR (KBr) 3075 (w), 2954 (s), 2905 (s), 2866 (m), 1610 (w), 1566 (m), 1476 (m), 1461 (w), 1437 (w), 1361 (w), 1261 (w), 1020 (w), 969 (w), 835 (w), 794 (s), 740 (w), 659 (w) cm^{-1}; MS (MALDI) m/z 1155.0 [M]$^+$; redox potentials (cyclic voltammetry) E_2^{ox} = −0.17, E_1^{ox} = −0.41, E_1^{red} = −1.47, E_2^{red} = −1.59 V vs Fc/Fc^+ (see also Figure S3 in SI).

2,6,13,17-Tetra-*tert*-butyl-4,15-di(4-*tert*-butyl-2,6-dimethylphenyl)quarteranthene (3b). The precursor **7b** (0.062 g, 0.050 mmol), DDQ (0.066 g, 0.29 mmol), and $Sc(OTf)_3$ (0.189 g, 0.38 mmol) were dissolved in anhydrous toluene (20 mL), and the mixture was refluxed for 84 h under an argon atmosphere. After the mixture was cooled to 0 °C, Et_3N (0.2 mL) and $N_2H_4{\cdot}H_2O$ (0.1 mL) were added, and the mixture was stirred for 10 min at 0 °C. The reaction mixture was poured onto hydrous (6%) alumina, and the product was eluted with toluene at −20 °C under argon flow to give **3b** as a bluish-black solid (0.035 g, 57%): mp (from toluene) >300 °C; IR (KBr) 3048 (w), 2954 (s), 2905 (s), 2866 (m), 1739 (w), 1606 (w), 1565 (m), 1479 (m), 1460 (w), 1393 (w), 1361 (m), 1226 (w), 968 (w), 868 (w), 793 (m), 754 (w), 659 (w) cm^{-1}; HRMS (ESI) m/z [M]$^+$ calcd for $C_{96}H_{86}$ 1238.6724, found 1238.6715.

Two-Photon Absorption Measurements. A two-photon absorption spectrum was measured by using the open-aperture Z-scan method.[48] The experimental setup was reported previously.[49] A femtosecond optical parametric amplifier (Spectra-Physics OPA-800) operating at a repetition rate of 1 kHz was used as light source to scan the excitation wavelength from 1680 to 2420 nm. The output beam of the parametric amplifier passed through a small iris to obtain a near-Gaussian spatial profile. The pulsewidth was measured at each wavelength by an autocorrelator (typically 110 fs in fwhm for Gaussian pulse) and used to calculate the peak optical intensity at the focal point I_0. The Rayleigh range z_R of the optical setup was 5−11 mm depending on the wavelengths employed. The sample solution (**3b** in CS_2, 1.1 mM) was held in a quartz cuvette (path length L = 1 mm), which is shorter than the z_R and satisfied the "optically thin" condition $L \ll z_R$.[48] The transmitted light through the sample was detected by an InGaAs photodiode attached to an integrating sphere. Measure-

dx.doi.org/10.1021/ja309599m | J. Am. Chem. Soc. 2013, 135, 1430−1437

ments were repeated at least four times by varying the incident laser power P_i in the range of 0.1−1 mW at each wavelength.

The recorded Z-scan traces were analyzed by the curve fitting procedure with the theoretical model of the transmittance of a spatially and temporally Gaussian pulse through two-photon absorptive media.[49] From the curve fitting the two-photon absorbance of the sample $q_0 = \alpha^{(2)} I_0 L$ was obtained, where $\alpha^{(2)}$ is the two-photon absorption coefficient. The proportionality relation of q_0 against I_0, therefore P_i, was confirmed, which verified that the observed signal surely arose from the two-photon absorption process. The I_0 employed was <200 GW cm^{-2}. Two-photon absorption spectrum (Figure 6) of the sample was obtained by repeating the measurement at each wavelength, where the linear absorption of both solute and solvent is absent.

Computational Details. All *ab initio* calculations were performed with the Gaussian 03 program[50] and the Molpro Version 2010.1 program package.[51] The molecular geometries of **1**, **2**, and **3** used for the CASSCF and NEVPT2 calculations were optimized at the UB3LYP/6-31G* level of theory. The aryl and *tert*-butyl substituent groups were replaced by hydrogen atoms.

Crystal Data for Compound 3a. T = 200(2) K, monoclinic, space group $P2_1/n$ (No. 14), a = 9.3333(7), b = 36.817(2), and c = 19.2308(14) Å, β = 96.9458(17)°, V = 6559.6(8) Å^3, Z = 4, R_1 (wR_2) = 0.0853 (0.2470) for 931 parameters and 14 923 independent reflections, GOF = 0.963. CCDC 903954.

Crystal Data for Compound 8. T = 200(2) K, triclinic, space group $P\bar{1}$ (No. 2), a = 9.7396(3), b = 19.3986(7), and c = 21.6326(8) Å, α = 77.6474(11), β = 89.1137(9), and γ = 84.1088(11)°, V = 3971.4(2) Å^3, Z = 2, R_1 (wR_2) = 0.0761 (0.1676) for 1133 parameters and 17 985 independent reflections, GOF = 1.022. CCDC 903955.

■ ASSOCIATED CONTENT

Supporting Information

Electronic absorption spectrum, cyclic voltammogram, and packing diagram of **3a**; ESR and variable-temperature ^{1}H NMR spectra of **3b**; computational odd electron density and spin density maps of **3**; details on the CASSCF and NEVPT2 calculations; CIF files of **3a** and **8**. This material is available free of charge via the Internet at http://pubs.acs.org.

■ AUTHOR INFORMATION

Corresponding Author

kubo@chem.sci.osaka-u.ac.jp

Notes

The authors declare no competing financial interest.

■ ACKNOWLEDGMENTS

This work was supported in part by a Grant-in-Aid for Scientific Research on Innovative Areas "Reaction Integration" (No. 2105) from the Ministry of Education, Culture, Sports, and Technology of Japan and by the ALCA Program of the Japan Science and Technology Agency (JST). A.K. acknowledges support from the JSPS Fellowship for Young Scientists. The authors thank Y. Aso and Y. Ie (the Institute of Science and Industrial Research, Osaka University) for the variable-temperature electronic absorption measurements and K. Wakabayashi (National Institute for Materials Science, NIMS) for fruitful discussions and helpful comments.

■ REFERENCES

(1) Novoselov, K. S.; Geim, A. K.; Morozov, S. V.; Jiang, D.; Zhang, Y.; Dubonos, S. V.; Grigorieva, I. V.; Firsov, A. A. *Science* **2004**, *306*, 666−669.

(2) Neto, A. H. C.; Guinea, F.; Peres, N. M. R.; Novoselov, K. S.; Geim, A. K. *Rev. Mod. Phys.* **2009**, *81*, 109−162.

(3) (a) Chen, L.; Hernandez, Y.; Feng, X.; Müllen, K. *Angew. Chem., Int. Ed.* **2012**, *51*, 7640−7654. (b) Enoki, T.; Takai, K.; Kiguchi, M. *Bull. Chem. Soc. Jpn.* **2012**, *85*, 249−264. (c) Morita, Y.; Suzuki, S.; Sato, K.; Takui, T. *Nat. Chem.* **2011**, *3*, 197−204.

(4) Tanaka, K.; Yamashita, S.; Yamabe, H.; Yamabe, T. *Synth. Met.* **1987**, *17*, 143−148.

(5) Fujita, M.; Wakabayashi, K.; Nakada, K.; Kusakabe, K. *J. Phys. Soc. Jpn.* **1996**, *65*, 1920−1923.

(6) Nakada, K.; Fujita, M.; Dresselhaus, G.; Dresselhaus, M. S. *Phys. Rev. B* **1996**, *54*, 17954−17961.

(7) Kobayashi, Y.; Fukui, K.; Enoki, T.; Kusakabe, K.; Kaburagi, Y. *Phys. Rev. B* **2005**, *71*, 193406-1−193406-4.

(8) Kobayahi, Y.; Fukui, K.; Enoki, T.; Kusakabe, K. *Phys. Rev. B* **2006**, *73*, 125415-1−125415-8.

(9) Sugawara, K.; Sato, T.; Souma, S.; Takahashi, T.; Suematsu, H. *Phys. Rev. B* **2006**, *73*, 045124-1−045124-4.

(10) Suenaga, K.; Koshino, M. *Nature* **2010**, *468*, 1088−1090.

(11) Hou, Z.; Wang, X.; Ikeda, T.; Huang, S.-F.; Terakura, K.; Boero, M.; Oshima, M.; Kakimoto, M.; Miyata, S. *J. Phys. Chem. C* **2011**, *115*, 5392−5403.

(12) Tao, C.; Jiao, L.; Yazyev, O. V.; Chen, Y.-C.; Feng, J.; Zhang, X.; Capaz, R. B.; Tour, J. M.; Zettl, A.; Louie, S. G.; Dai, H.; Crommie, M. F. *Nat. Phys.* **2011**, *7*, 616−620.

(13) Pan, M.; Girão, E. C.; Jia, X.; Bhaviripudi, S.; Li, Q.; Kong, J.; Meunier, V.; Dresselhaus, M. S. *Nano Lett.* **2012**, *12*, 1928−1933.

(14) Barone, V.; Hod, O.; Scuseria, G. E. *Nano Lett.* **2006**, *6*, 2748−2754.

(15) Son, Y.-W.; Cohen, M. L.; Louie, S. G. *Nature* **2006**, *444*, 347−349.

(16) Yang, X. Y.; Dou, X.; Rouhanipour, A.; Zhi, L.; Räder, H. J.; Müllen, K. *J. Am. Chem. Soc.* **2008**, *130*, 4216−4217.

(17) Cai, J.; Ruffieux, P.; Jaafar, R.; Bieri, M.; Braun, T.; Blankenburg, S.; Muoth, M.; Seitsonen, A. P.; Saleh, M.; Feng, X.; Müllen, K.; Fasel, R. *Nature* **2010**, *466*, 470−473.

(18) Chen, Z.; Lin, Y.-M.; Rooks, M. J.; Avouris, P. *Physica E* **2007**, *40*, 228−232.

(19) Han, M. Y.; Özyilmaz, B.; Zhang, Y.; Kim, P. *Phys. Rev. Lett.* **2007**, *98*, 206805-1−206805-4.

(20) Kosynkin, D. V.; Higginbotham, A. L.; Sinitskii, A.; Lomeda, J. R.; Dimiev, A.; Price, B. K.; Tour, J. M. *Nature* **2009**, *458*, 872−876.

(21) Jiao, L.; Wang, X.; Diankov, G.; Wang, H.; Dai, H. *Nat. Nanotechnol.* **2010**, *5*, 321−325.

(22) Very recently Hong et al. have prepared zigzag edges by the direct chemical functionalization of graphene, which allows the direct observation of room temperature magnetic ordering in 30 Å wide ZGNRs. Hong, J.; Bekyarova, E.; Liang, P.; de Heer, W. A.; Haddon, R. C.; Khizroev, S. *Sci. Rep.* **2012**, *2*, 624.

(23) Stein, S. E.; Brown, R. L. *J. Am. Chem. Soc.* **1987**, *109*, 3721−3729.

(24) Bendikov, M.; Duong, H. M.; Starkey, K.; Houk, K. N.; Carter, E. A.; Wudl, F. *J. Am. Chem. Soc.* **2004**, *126*, 7416−7417.

(25) Hachmann, J.; Dorando, J. J.; Avilés, M.; Chan, G. K.-L. *J. Chem. Phys.* **2007**, *127*, 134309-1−134309-9.

(26) Moscardó, F.; San-Fabián, E. *Chem. Phys. Lett.* **2009**, *480*, 26−30.

(27) Konishi, A.; Hirao, Y.; Nakano, M.; Shimizu, A.; Botek, E.; Champagne, B.; Shiomi, D.; Sato, K.; Takui, T.; Matsumoto, K.; Kurata, H.; Kubo, T. *J. Am. Chem. Soc.* **2010**, *132*, 11021−11023.

(28) Lambert, C. *Angew. Chem., Int. Ed.* **2010**, *50*, 1756−1758.

(29) For a recent review, see: Sun, Z.; Ye, Q.; Chunyan, C.; Wu, J. *Chem. Soc. Rev.* **2012**, *41*, 7857−7889.

(30) Eckert, A.; Tomaschek, R. *Monatsh. Chem.* **1918**, *39*, 839−864.

(31) Clar, E.; Kelly, W.; Wright, J. W. *J. Chem. Soc.* **1954**, 1108−1111.

(32) The formation of multiple bonds in one step is categorized as *time and space integration*. Suga, S.; Yamada, D.; Yoshida, J. *Chem. Lett.* **2010**, *39*, 404−406.

(33) Imamoto, T.; Takiyama, N.; Nakamura, K.; Hatajima, T.; Kamiya, Y. *J. Am. Chem. Soc.* **1989**, *111*, 4392−4398.

(34) Li, Y.; Wang, Z. *Org. Lett.* **2009**, *11*, 1385−1387.

(35) Li, J.; Zhang, K.; Zhang, X.; Huang, K.-W.; Chi, C.; Wu, J. *J. Org. Chem.* **2010**, *75*, 856−863.
(36) Döhnert, D.; Koutecký. *J. Am. Chem. Soc.* **1980**, *102*, 1789−1796.
(37) In a multiconfigurational scheme, the mixing of a doubly excited configuration $^1\Phi_{H,H\rightarrow L,L}$ with a ground-state configuration $^1\Phi_{H,H}$ represents uncoupling of electron pair, and hence the occupation number of LUMO is a direct computational measure of the amount of the singlet biradical character. A perfect biradical is characterized by occupation numbers of 1.0 in HOMO and LUMO, whereas a perfect closed-shell molecule possesses occupation numbers of 2.0 and 0.0 in HOMO and LUMO, respectively.
(38) Kruszewski, J.; Krygowski, T. M. *Tetrahedron Lett.* **1972**, *13*, 3839−3842.
(39) Krygowski, T. M. *J. Chem. Inf. Comput. Sci.* **1993**, *33*, 70−78.
(40) Pisani, L.; Chan, J. A.; Montanari, B.; Harrison, N. M. *Phys. Rev. B* **2007**, *75*, 064418-1−064418-9.
(41) Similar signal broadening is observed in nitronyl nitroxide biradicals with a similar $\Delta E_{S\text{-}T}$. (a) Ullman, E. F.; Osiecki, J. H.; Boocock, G. B.; Darcy, R. *J. Am. Chem. Soc.* **1972**, *94*, 7049−7059. (b) Ziessel, R.; Stroh, C.; Heise, H.; Köhler, F. H.; Turek, P.; Claiser, N.; Souhassou, M.; Lecomte, C. *J. Am. Chem. Soc.* **2004**, *126*, 12604−12613.
(42) Intensity of the forbidden half-field signal is proportional to r^{-6} (r is an interspin distance). Eaton, S. S.; More, K. M.; Sawant, B. M.; Eaton, G. R. *J. Am. Chem. Soc.* **1983**, *105*, 6560−6567.
(43) Meyer, Y. H.; Astier, R.; Leclercq, J. M. *J. Chem. Phys.* **1972**, *56*, 801−815.
(44) Angeli, C.; Pastore, M.; Cimiraglia, R. *Theor. Chem. Acc.* **2007**, *117*, 743−754.
(45) Although the origin of the signal around 1900 nm in the TPA spectrum is still unclear, a vibronic transition may cause some TPA transition intensity.
(46) Lee, Y. H.; Kim, S. G.; Tománek, D. *Phys. Rev. Lett.* **1997**, *78*, 2393−2396.
(47) Kawai, T.; Miyamoto, Y.; Sugino, O.; Koga, Y. *Phys. Rev. B* **2000**, *62*, R16349−R16352.
(48) Sheik-Bahae, M.; Said, A. A.; Wei, T.-H.; Hagan, D. J.; Van Stryland, E. W. *IEEE J. Quantum Electron.* **1990**, *26*, 760−769.
(49) Kamada, K.; Matsunaga, K.; Yoshino, A.; Ohta, K. *J. Opt. Soc. Am. B* **2003**, *20*, 529−537.
(50) Frisch, M. J.; Trucks, G. W.; Schlegel, H. B.; Scuseria, G. E.; Robb, M. A.; Cheeseman, J. R.; Montgomery, J. A., Jr.; Vreven, T.; Kudin, K. N.; Burant, J. C.; Millam, J. M.; Iyengar, S. S.; Tomasi, J.; Barone, V.; Mennucci, B.; Cossi, M.; Scalmani, G.;Rega, N.; Petersson, G. A.; Nakatsuji, H.; Hada, M.; Ehara, M.; Toyota, K.; Fukuda,R.; Hasegawa, J.; Ishida, M.; Nakajima, T.; Honda, Y.; Kitao, O.; Nakai, H.; Klene,M.; Li, X.; Knox, J. E.; Hratchian, H. P.; Cross, J. B.; Adamo, C.; Jaramillo, J.;Gomperts, R.; Stratmann, R. E.; Yazyev, O.; Austin, A. J.; Cammi, R.; Pomelli, C.;Ochterski, J. W.; Ayala, P. Y.; Morokuma, K.; Voth, G. A.; Salvador, P.; Dannenberg,J. J.; Zakrzewski, V. G.; Dapprich, S.; Daniels, A. D.; Strain, M. C.; Farkas, O.;Malick, D. K.; Rabuck, A. D.; Raghavachari, K.; Foresman, J. B.; Ortiz, J. V.; Cui, Q.; Baboul, A. G.; Clifford, S.; Cioslowski, J.; Stefanov, B. B.; Liu, G.; Liashenko, A.; Piskorz, P.; Komaromi, I.; Martin, R. L.; Fox, D. J.; Keith, T.; Al-Laham, M. A.; Peng, C. Y.; Nanayakkara, A.; Challacombe, M.; Gill, P. M. V.; Johnson, B.; Chen, W.; Wong, M. W.; Gonzales, C.; Pople, J. A. *Gaussian 03*, revision D.01; Gaussian, Inc.: Pittsburgh, PA, 2003.
(51) Werner, H.-J.; Knowles, P. J.; Knizia, G.; Manby, F. R.; Schütz, M.; Celani, P.; Korona, T.; Lindh, R.; Mitrushenkov, A.; Rauhut, G.; Shamasundar, K. R.; Adler, T. B.; Amos, R. D.; Bernhardsson, A.; Berning, A.; Cooper, D. L.; Deegan, M. J. O.; Dobbyn, A. J.; Eckert, F.; Goll, E.; Hampel, C.; Hesselmann, A.; Hetzer, G.; Hrenar, T.; Jansen, G.; Köppl, C.; Liu, Y.; Lloyd, A. W.; Mata, R. A.; May, A. J.; McNicholas, S. J.; Meyer, W.; Mura, M. E.; Nicklaß, A.; O'Neill, D. P.; Palmieri, P.; Peng, D.; Pflüger, K.; Pitzer, R.; Reiher, M.; Shiozaki, T.; Stoll, H.; Stone, A. J.; Tarroni, R.; Thorsteinsson, T.; Wang M. *MOLPRO: a package of ab initio programs*, version 1; 2010.